

# Absorbing Phase Transitions and Dynamic Freezing in Running Active Matter Systems

Charles Reichhardt and Cynthia J. Olson Reichhardt,\*

Received Xth XXXXXXXXXXXX 20XX, Accepted Xth XXXXXXXXXXXX 20XX

First published on the web Xth XXXXXXXXXXXX 200X

DOI: 10.1039/b000000x

We examine a two-dimensional system of sterically repulsive interacting disks where each particle runs in a random direction. This system is equivalent to a run-and-tumble dynamics system in the limit where the run time is infinite. At low densities, we find a strongly fluctuating state composed of transient clusters. Above a critical density that is well below the density at which non-active particles would crystallize, the system can organize into a drifting quiescent or frozen state where the fluctuations are lost and large crystallites form surrounded by a small density of individual particles. Although all the particles are still moving, their paths form closed orbits. The average transient time to organize into the quiescent state diverges as a power law upon approaching the critical density from above. We compare our results to the random organization observed for periodically sheared systems that can undergo an absorbing transition from a fluctuating state to a dynamical non-fluctuating state. In the random organization studies, the system organizes to a state in which the particles no longer interact; in contrast, we find that the randomly running active matter organizes to a strongly interacting dynamically jammed state. We show that the transition to the frozen state is robust against a certain range of stochastic fluctuations. We also examine the effects of adding a small number of pinned particles to the system and find that the transition to the frozen state shifts to significantly lower densities and arises via the nucleation of faceted crystals centered at the obstacles.

## 1 Introduction

Nonequilibrium collections of interacting particles often form strongly fluctuating or turbulent states and can exhibit nonequilibrium phase transitions between distinct dynamical regimes<sup>1–3</sup>. Examples of such systems include sheared colloids<sup>4–7</sup>, turbulent liquid crystals<sup>8</sup>, granular matter<sup>9,10</sup>, driven vortex matter in type-II superconductors<sup>11,12</sup>, and active matter or self-driven particle assemblies<sup>13–16</sup>. In certain cases a nonequilibrium transition can be identified to occur between a fluctuating state and a quiescent state in which fluctuations are almost completely absent but the system is still out of equilibrium or even in motion; here, the system can become dynamically trapped into an absorbing phase<sup>1,2</sup>. The absence of fluctuations in the absorbing or quiescent state makes it impossible for the system to escape from this state.

Recently, periodically sheared dilute colloidal suspensions were shown to be an outstanding example of a system exhibiting the hallmark features of a transition into an absorbing phase<sup>4–7</sup>. Thermal fluctuations are negligible in this system, so the dynamics is governed by collisions between the particles. Both numerical and experimental studies compared the position of the colloidal particles at the beginning and

end of each shear cycle. This protocol permits the identification of two distinct dynamical regimes. In the fluctuating or irreversible state, the particles are at different locations at the beginning and end of each cycle, and perform an anisotropic random walk over the course of many cycles. In the reversible state, particles return to the same position after each cycle and fluctuations vanish when the particles organize into a configuration that prevents particle-particle collisions from occurring<sup>4,5</sup>. For fixed particle density, the reversible state appears below a critical oscillatory shear amplitude  $\gamma_c$ , while at high shear amplitudes the system remains in the fluctuating state. When the periodic shear is first applied, the system always starts in an irreversible fluctuating state, but after a number of cycles it either organizes into a steady irreversible state or reaches a reversible quiescent state. As  $\gamma_c$  is approached, the number of cycles or the total time  $\tau$  required for the system to reach one of these states diverges as a power law  $\tau \propto |\gamma - \gamma_c|^{-\nu_{||}}$ , with  $\nu_{||} \approx 1.35$  in two-dimensional (2D) simulations and  $\nu_{||} \approx 1.5$  in three-dimensional (3D) experiments<sup>5</sup>. Major classes of absorbing phase transitions include directed percolation<sup>1,17,18</sup> and conserved directed percolation<sup>2,18</sup>, which have predicted exponents in 2D of  $\nu_{||} = 1.295$  and  $\nu_{||} = 1.225$ , respectively.

In the colloidal system the absorbing state is characterized by the organization of the particles into a random pattern in which they do not interact with each other, leading the transi-

Theoretical Division, Los Alamos National Laboratory, Los Alamos, New Mexico 87545, USA. Fax: 1 505 606 0917; Tel: 1 505 665 1134; E-mail: [cjrx@lanl.gov](mailto:cjrx@lanl.gov)

tion to be termed “random organization”<sup>5,18</sup>. A similar periodic drive protocol has been used to analyze other nonequilibrium systems, such as periodically driven superconducting vortices<sup>11,12</sup> and granular media<sup>18–20</sup>, by identifying the transient time required to transition from irreversible to reversible flow. Other studies have shown that a transition from an irreversible to a reversible state can occur even when the reversible state is strongly interacting, such as in jammed solids<sup>21–24</sup>, and in some cases this transition is associated with a power law divergence of a time scale, indicative of a critical point<sup>21,22,24</sup>.

Another type of nonequilibrium systems is self-driven particles or active matter<sup>13,16,25</sup>, which include swimming bacteria undergoing run-and-tumble dynamics<sup>26–30</sup>, flocking particles<sup>31,32</sup>, pedestrian motion<sup>33</sup>, and self-driven colloidal particles<sup>34–40</sup>. One class of active matter is run-and-tumble self-driven particles, which move or run in a randomly chosen direction for a period of time before undergoing a tumbling event and then moving in a freshly chosen random direction. Run-and-tumble dynamics have been used to model systems such as swimming bacteria<sup>26–29,38</sup>. Another active matter class is active Brownian particles such as Janus colloids. Here each particle is self-driven but its direction of motion slowly diffuses<sup>34,36–39</sup>. When the active particles have additional steric interactions, a transition can occur from a uniform liquid state to a phase-separated state consisting of high density clusters separated by a low density dilute gas<sup>29,37–48</sup>. The high density state can be characterized as having glass<sup>43,46</sup> or crystalline<sup>37,39,42,44,45</sup> order. The cluster structures are only transient and exhibit fluctuations in which the clusters can break up and reform over time, as observed in recent experiments where the clusters were described as “living crystals”<sup>37,39</sup>. When the particle density is increased, the system eventually enters a dense jammed state in which slow rearrangements of the particles can still occur due to their activity<sup>41,49</sup>.

Here we investigate whether active matter systems can exhibit absorbing transitions similar to the random organization from a strongly fluctuating state to a dynamically frozen steady state. Active matter systems such as run-and-tumble and active Brownian particles are usually modeled by including a stochastic term either in the randomization of the running direction during a tumble or in the slow diffusion of the running direction, respectively. Deterministic dynamics can occur in certain limits, such as infinite run lengths in the run-and-tumble systems, or in the absence of a diffusive term in the active Brownian particles. In these deterministic limits, each particle moves in a fixed direction but can still interact with other particles to create a fluctuating state. When the dynamics is free of stochastic fluctuations, as in recent numerical studies of binary rotating cross-shaped particles, it was shown that after some time particles with different rotation directions could organize into a phase-separated state<sup>50</sup>. This

system is similar to the random organization studies in that the particles are initially in a fluctuating state and after some time either settle into a dynamically frozen state or remain in a continuously fluctuating state<sup>5</sup>. Other studies of growing actin filaments found evidence of organization into a quiescent absorbing state consisting of spiral patterns<sup>14,15</sup>.

We consider run-and-tumble sterically repulsive disks in the limit where the particles have an infinite run time. The initial positions of the particles and the run directions are selected randomly. At low density the system forms a strongly fluctuating state containing short-lived clusters; however, above a critical density  $\phi_c$  the system can organize into a non-fluctuating or quiescent state comprised of a single drifting crystalline cluster surrounded by a number of individual particles that are traveling in closed orbits. By starting from the high density limit and decreasing the density to  $\phi_c$ , we find that the time required for the system to organize to a frozen state increases with decreasing  $\phi$  and diverges as a power law at  $\phi_c$  with  $\nu_{||} = 1.21 \pm 0.3$ , consistent with the exponents found in the random organization system and conserved directed percolation. We show that the transition is robust against the addition of some thermal noise; however, at high enough noise it is no longer possible for a completely dynamically frozen state to form. When we add a small number of pinned particles, we find that the system can organize to a dynamically frozen pinned state at densities well below the obstacle-free  $\phi_c$ . The pinned frozen states contain faceted hexagonal crystals that are centered at the obstacle sites.

## 2 Simulation and System

We consider a 2D system of size  $L \times L$  with periodic boundary conditions in the  $x$  and  $y$ -directions. The sample contains  $N$  active disks with radius  $R_d$  that interact with each other via a steric harmonic repulsion. The disk density  $\phi = \pi N R_d^2 / L^2$  is the total fraction of the sample area covered by the disks. A sample filled with inactive disks crystallizes into a triangular lattice at a density of  $\phi \approx 0.9$ . The motion of an individual disk  $i$  located at  $\mathbf{r}_i$  is obtained by integrating the overdamped equations of motion,

$$\eta \frac{d\mathbf{r}_i}{dt} = \mathbf{F}_i^m + \mathbf{F}_i^s. \quad (1)$$

Here  $\eta$  is the damping constant,  $\mathbf{F}_i^m = F_d \hat{\mathbf{m}}_i$  is the motor force, and  $\mathbf{F}_i^s$  describes the particle-particle interactions. The motor force consists of a fixed force  $F_d$  applied in a fixed direction  $\hat{\mathbf{m}}_i$  that is randomly selected for each disk at the beginning of the simulation and then never changed. For run-and-tumble dynamics this corresponds to an infinite run length, while for active Brownian particles it would correspond to zero rotational diffusion of the particle motion. The steric disk-disk repulsion is  $\mathbf{F}_i^s = \sum_{i \neq j}^N k(2R_d - |\mathbf{r}_{ij}|)\Theta(2R_d -$

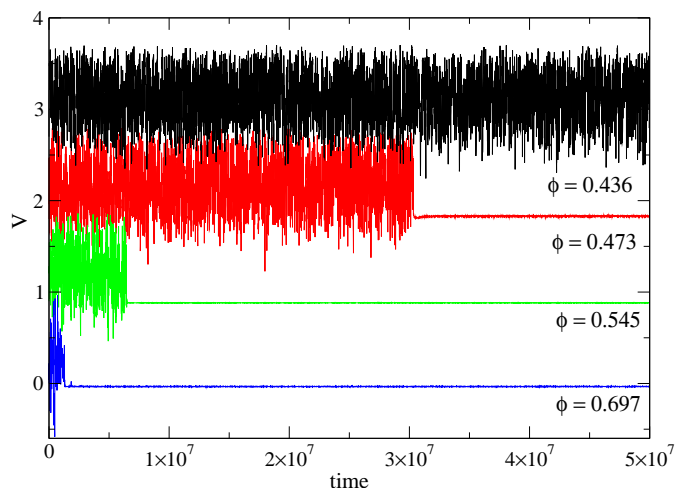


**Fig. 1** The velocity fluctuations  $V(t)$  of a single probe particle driven in the  $x$  direction for disk densities  $\phi = 0.436, 0.473, 0.545,$  and  $0.697$ , from top to bottom. The curves have been vertically shifted for clarity. For  $\phi = 0.473$  and above, there is a transition from a strongly fluctuating state to a non-fluctuating state after an average time that decreases with increasing  $\phi$ . Below a critical  $\phi_c$ , the system remains in the fluctuating state.

$|\mathbf{r}_{ij}| \hat{\mathbf{r}}_{ij}$ , where  $\mathbf{r}_{ij} = \mathbf{r}_i - \mathbf{r}_j$  and  $\hat{\mathbf{r}}_{ij} = \mathbf{r}_{ij}/|\mathbf{r}_{ij}|$ . We set  $R_d = 0.5$  and select parameters  $k = 20$  and  $F_d = 0.5$  such that disks cannot squeeze past a jammed configuration due to the driving force. Pinned particles or obstacles are introduced in the form of  $N_p$  immobile disks that have the same steric repulsive interactions as the mobile disks. Their density is given by  $\phi^p = N_p \pi R_d^2 / L^2$ .

### 3 Results

To characterize the activity in the system, we measure the velocity fluctuations  $V(t)$  at varied  $\phi$  of a single probe particle  $p$  moving in the positive  $x$ -direction, where  $V(t) = \dot{x}_p(t)$  and  $\hat{\mathbf{m}}_p = \hat{\mathbf{x}}$ . Figure 1 shows a series of  $V(t)$  curves taken at  $\phi = 0.436, 0.473, 0.545,$  and  $0.697$ . At  $\phi = 0.697$ , the system starts in a fluctuating state with transient clusters or living crystals, but after  $1.5 \times 10^6$  simulation time steps the fluctuations almost completely vanish and  $V \approx 0$ . The other particles in the system exhibit the same behavior as the probe particle, and have the same transition to a nonfluctuating velocity occurring at the same time. The time required to reach the non-fluctuating state is labeled  $\tau$ . For  $\phi = 0.545$  we find the same transition to a non-fluctuating state but  $\tau$  is larger, and as  $\phi$  is further decreased  $\tau$  continues to increase as shown for  $\phi = 0.473$ . For  $\phi < 0.46$ , the system never reaches a non-fluctuating state even for extremely long simulation times.

In any individual simulation at a given value of  $\phi$  there is

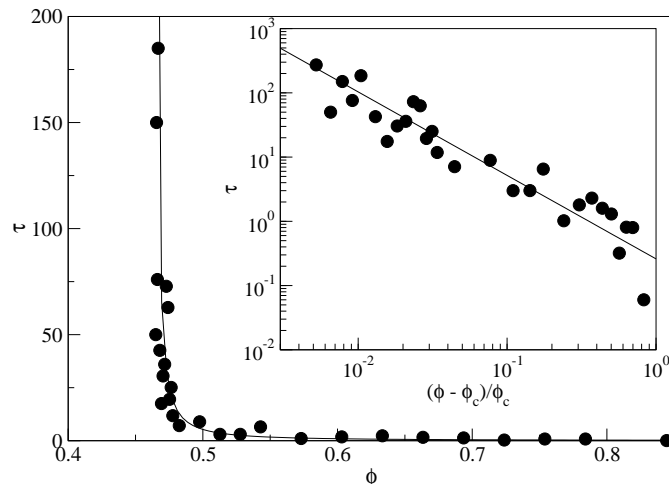


**Fig. 2** The transient time  $\tau$  to reach a dynamically frozen state vs  $\phi$ . The solid line is a fit to  $\tau = (\phi - \phi_c)^{-\nu_{||}}$ , with  $\phi_c = 0.462$  and  $\nu_{||} = 1.21$ . The  $\tau$  axis is divided by  $10^6$  simulation time steps. Inset: The same data on a log-log plot showing the power law fit.

some variation in the value of  $\tau$  when different random initial conditions are chosen; however, the average value of  $\tau$  robustly increases with decreasing  $\phi$  and we find that  $\tau$  diverges at a critical density  $\phi_c$ . In Fig. 2 we plot  $\tau$  versus  $\phi$ , where the solid line is a fit to the form  $\tau = (\phi - \phi_c)^{-\nu_{||}}$  using  $\phi_c = 0.462$  and  $\nu_{||} = 1.21$ . The inset of Fig. 2 shows a log-log plot of  $\tau$  versus  $(\phi - \phi_c)/\phi_c$  fit using  $\nu_{||} = 1.21 \pm 0.06$ . The diverging time scale for the transition from a fluctuating state to a dynamically frozen state is very similar to what is observed in the periodically sheared colloidal system, where a diverging time scale appears at a critical shear amplitude with exponent  $\nu_{||} = 1.33$  measured in 2D colloidal simulations<sup>5</sup>. Other simulations of a diverging time scale at the transition to a dynamically frozen state for a periodically sheared disk system give  $\nu_{||} = 1.3$ <sup>18</sup>. These exponents are close to the values  $\nu_{||} = 1.295$  and  $\nu_{||} = 1.225$  expected for 2D directed percolation (DP)<sup>17,18</sup> and 2D conserved directed percolation (CDP)<sup>2,18</sup>, respectively. Our regression fit gives a value of  $\nu_{||}$  closer to the expected value for 2D CDP; however, our results are not accurate enough to positively distinguish between DP and CDP. We note that in our system the particle number is conserved.

The non-fluctuating state in the random organization system consists of particles that are moving but that have organized into a dynamic configuration in which they no longer collide with one another<sup>5</sup>. In contrast, we find that the active matter system organizes into a non-fluctuating cluster where most of the particles are in contact with each other. We note that the cluster state is still dynamical since it continues to drift through the system in a direction determined by the net sum of

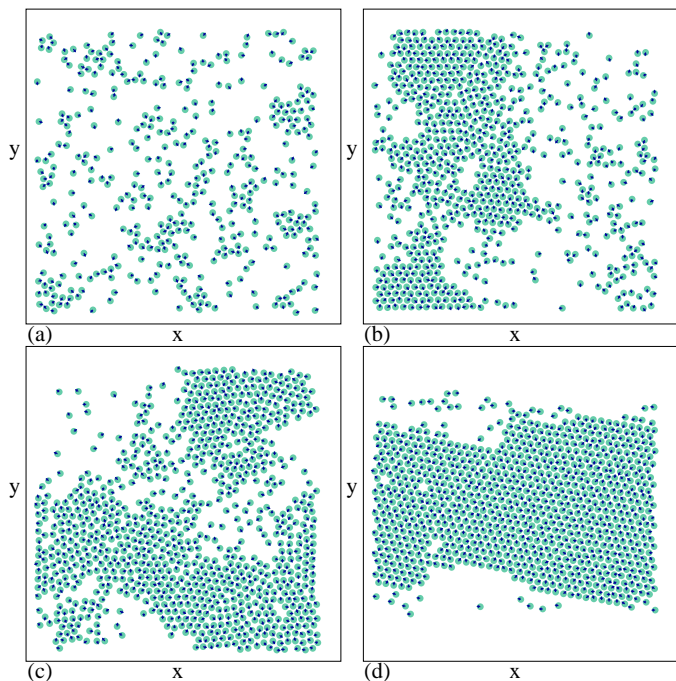


**Fig. 3** Snapshots of disk positions where the arrows indicate the direction of the motor force for each disk. (a) The fluctuating state at  $\phi = 0.242$  where only small transient clusters form. (b) The fluctuating state at  $\phi = 0.436$  where a living crystal cluster forms. (c) The transient fluctuating state at  $\phi = 0.545$ . (d) The dynamically frozen steady state at  $\phi = 0.545$ , where a single large crystal forms and drifts through the system.

the motor forces of all the particles contained in the cluster. In Fig. 3 we illustrate the disk positions along with the direction of the motor force for each disk. Figure 3(a) shows a fluctuating state for  $\phi < \phi_c$  at  $\phi = 0.242$ . At this density the system forms transient clusters that change rapidly. At  $\phi = 0.436$  in Fig. 3(b), below  $\phi_c$ , the system phase separates into living crystal clumps with triangular ordering which break apart over time, as observed in other active matter studies<sup>37,39,42–46</sup>.

In Fig. 3(c) we illustrate the transient active fluctuating state at  $\phi = 0.545$  which is above  $\phi_c$ , while in Fig. 3(d) we show the dynamically frozen steady state that forms at later times. In the frozen state, the disks form a single crystalline structure that does not change, and the particles within the cluster maintain the same neighbors over time. The entire cluster slowly drifts across the sample as a function of time, while the disks that are not part of the cluster follow closed orbits which repeat over time due to the periodic boundary conditions. The system can be regarded as organizing not into a random state but rather into a jammed non-fluctuating state. Due to the absence of fluctuations, the particles in the cluster remain trapped in this configuration even though all of the particles are still subject to a motor force and the entire cluster assembly is moving as a rigid object. The number of configurations that produce frozen states increases with increasing  $\phi$ , so the average time  $\tau$  required for the particles to find a dynamically frozen state decreases with increasing  $\tau$  as shown in Figs. 1,2.

In order to better understand the stability of the frozen states, we color the particles according to the net component of the motor force along the  $y$  direction. Particles that have a net motion in the positive  $y$  direction are plotted with a dark color and a light arrow, while particles that have a net motion in the negative  $y$  direction are drawn with a light color and a dark arrow. Figure 4(a) shows the configuration at  $\phi = 0.545$  in the fluctuating state where the system forms transient living crystals. A stable cluster can form when groups of particles come together that have on average opposite swimming directions. In Fig. 4(b) we illustrate the dynamically frozen steady state at  $\phi = 0.545$ . Particles in the lower half of the cluster are generally moving in the positive  $y$  direction, while particles in the upper half of the cluster are generally moving in the negative  $y$ -direction, so that the cluster can be regarded as a blocked or jammed state in which the particles can no longer move past one another. Figure 4(c) shows the dynamically frozen steady state at  $\phi = 0.73$ , where again we find a similar phenomenon in which the lower half of the cluster is moving against the upper half. As the density increases, the size of the cluster grows until eventually the system forms a triangular lattice with embedded voids, as shown in Fig. 4(d) for the dynamically frozen steady state at  $\phi = 0.848$ . At these

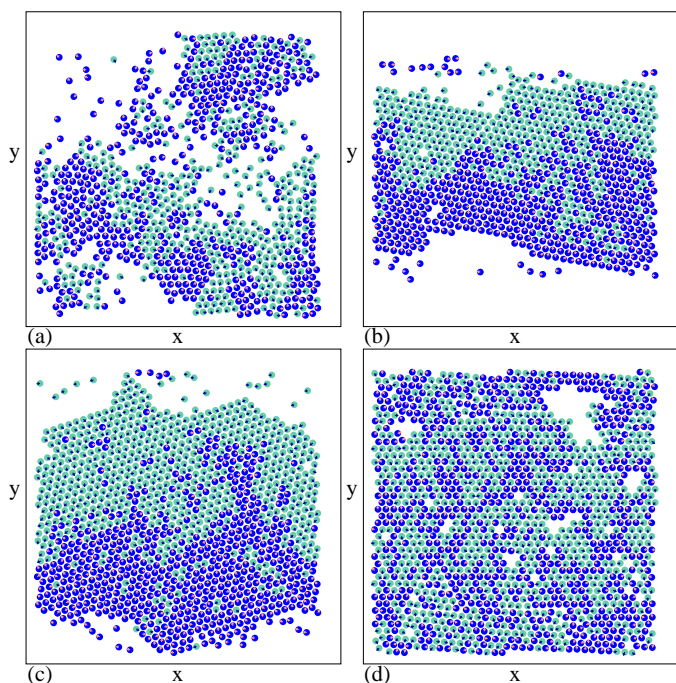


**Fig. 4** Snapshots of the disk positions where the arrows indicate the direction of the motor force for each disk. Dark particles with light arrows have a net motion in the positive  $y$  direction; light particles with dark arrows have a net motion in the negative  $y$  direction. (a) The transient fluctuating state at  $\phi = 0.545$ . (b) The dynamically frozen steady state at  $\phi = 0.545$  where a single large cluster forms. Particles in the lower half of the cluster are generally moving in the positive  $y$  direction, while particles in the upper half of the cluster are generally moving in the negative  $y$  direction, creating a jammed state. (c) The dynamically frozen steady state at  $\phi = 0.73$ . (d) The dynamically frozen steady state at  $\phi = 0.848$ , where a single large crystalline structure forms that drifts through the system.

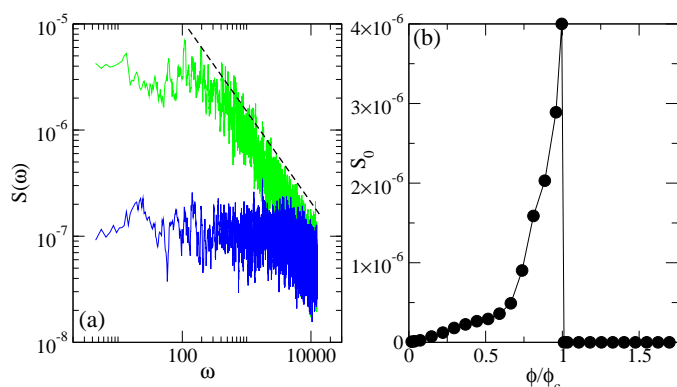


**Fig. 5** (a) Power spectrum  $S(\omega)$  of the time series  $V(t)$  of the velocity fluctuations for  $\phi/\phi_c = 0.0732$  (lower curve) and  $\phi/\phi_c = 0.988$  (upper curve). The dashed line is a fit to  $1/f^\alpha$  with  $\alpha = 1.0$ . (b) The noise power  $S_0$  vs  $\phi/\phi_c$  obtained by integrating  $S(\omega)$  over a fixed interval of  $\omega$ .  $S_0$  peaks just below  $\phi_c$ .

high densities the frozen states no longer have the same clear top/bottom asymmetry features and the crystalline state can be stabilized with more random up/down particle arrangements. Eventually at  $\phi = 0.9$  the system would naturally crystallize on its own even in the absence of motor forces. Since the number of random configurations that lead to a stable crystalline state increases as  $\phi = 0.9$  is approached from below, the time  $\tau$  required to reach an absorbing state decreases with increasing  $\phi$  above  $\phi_c$ .

The transient times  $\tau$  generally increase for increasing system size  $L$ ; however, the value of  $\phi_c$  does not shift. The dynamically frozen steady states are likely affected by the periodic boundary conditions, which limit the total number of possible configurations. In any real experiments performed with active matter, the system will also be bounded and have a limit on the number of possible configurations, so we expect that the transition to a dynamically frozen steady state that we find can be readily observed in experiment.

## 4 Noise Fluctuations

In the sheared colloidal system of Ref.<sup>5</sup>, two transient times were observed. The first is the time  $\tau$  required for the system to settle into the non-fluctuating state on the low shear amplitude side of transition, and the second is the time required for the system to settle into a steady fluctuating state as the critical shear amplitude is approached from above<sup>5</sup>. In our system, for  $\phi < \phi_c$  we do not find a clear transient signature for the settling of the fluctuations into a steady fluctuating state; however, we can measure the changes in the velocity fluctuations upon approaching  $\phi_c$  from below. In Fig. 5(a) we plot power spectra obtained from the time series of the velocity fluctuations,  $S(\omega) = |\int V(t)e^{-i\omega t} dt|^2$  at  $\phi/\phi_c = 0.0732$  and  $\phi/\phi_c = 0.988$ . Here we find that upon approaching  $\phi_c$  from below, the noise characteristic changes from white at low  $\phi/\phi_c$  to a  $1/f^\alpha$  form close to the transition, with a large increase in the noise power at low frequencies. The solid line in Fig. 5(a) is a fit with  $\alpha = 1.0$ .

We can further characterize the noise by measuring the noise power  $S_0$ , obtained by integrating  $S(\omega)$  over a range of low frequencies<sup>51–53</sup>. In Fig. 5(b) we plot  $S_0$  versus  $\phi/\phi_c$  showing that the noise power peaks just below  $\phi_c$ . The noise measurements taken in the frozen steady state for  $\phi > \phi_c$  show very low noise power due to the lack of fluctuations. A peak in the noise power has previously been proposed to indicate the presence of a critical point in both equilibrium<sup>54</sup> and nonequilibrium systems<sup>55</sup>. The increase in the low frequency noise power indicates that the fluctuations are occurring on larger length scales and thus take longer time scales to occur. This is correlated with the living crystals becoming longer lived as  $\phi_c$  is approached. Once the living crystal structure becomes large enough, the system can find a dynamically



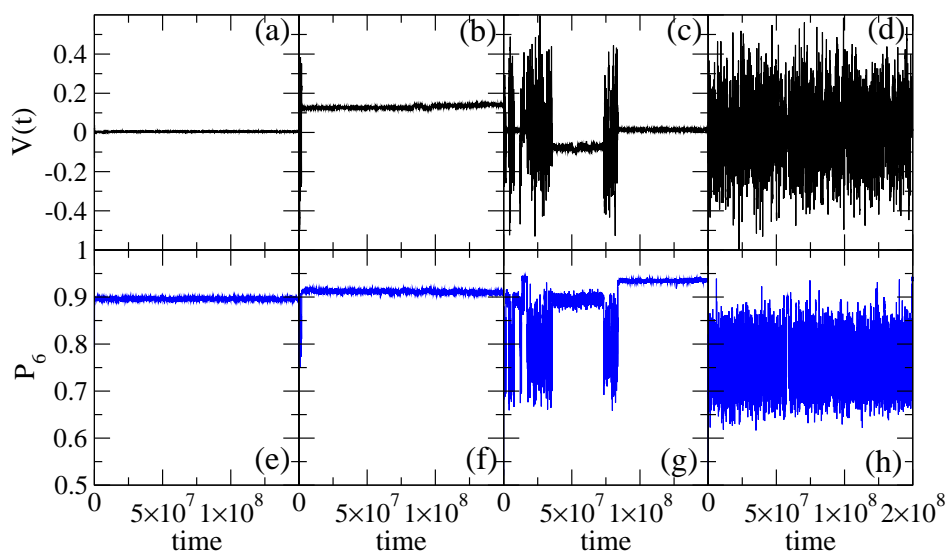


**Fig. 6** (a,b,c,d)  $V(t)$  for a system at  $\phi/\phi_c = 1.43$  where stochastic noise is added in the form of thermal kicks of magnitude  $F^T = 0$  (a), 2.0 (b), 6.0 (c), and 9.0 (d). (e,f,g,h) The corresponding fraction of particles with six-fold neighbors  $P_6(t)$  for a system at  $\phi/\phi_c = 1.43$  and  $F^T = 0$  (e), 2.0 (f), 6.0 (g), and 9.0 (h).

frozen configuration and then remains trapped in that state.

## 5 Thermal Noise

We next consider the robustness of the transition into the dynamically frozen state in the presence of stochastic noise, introduced by adding Langevin kicks  $\mathbf{F}^T$  to the equations of motion with the following properties:  $\langle \mathbf{F}^T(t) \rangle = 0$  and  $\langle F_i^T(t) F_j^T(t') \rangle = 2\eta k_B T \delta_{ij} \delta(t - t')$ . In the absence of other particles or a motor force, these kicks induce a random motion of an individual particle. We find that close-packed crystals at  $\phi = 0.9$  with no motor force thermally disorder when  $F^T > 8.0$ . In general we find that for  $\phi > \phi_c$ , a transition to the dynamically frozen state still occurs provided that the thermal fluctuations are small enough; however, even at higher values of  $F^T$  we observe a distinct difference in the dynamics of the system for  $\phi > \phi_c$  compared to  $\phi < \phi_c$ .

In Fig. 6(a-d) we plot  $V(t)$  for a system at  $\phi/\phi_c = 1.43$  with different thermal noise levels  $F^T = 0.0, 2.0, 6.0,$  and  $9.0$ . In Fig. 6(e-h) we show the corresponding fraction of six-fold coordinated particles  $P_6(t)$  vs time. To compute  $P_6$ , we find  $z_i$ , the number of neighbors of particle  $i$ , from a Voronoi construction, and then obtain  $P_6 = N^{-1} \sum_i \delta(z_i - 6)$ . In the frozen cluster state, most of the particles have six neighbors so  $P_6 \approx 0.9$  as shown in Fig. 6(e) for  $F^T = 0$ , where the velocity fluctuations are also small as indicated in Fig. 6(a). The transition to the quasistatic cluster state remains robust even for finite  $F^T$ , as shown in Fig. 6(b,f) at  $F^T = 2.0$  where the system rapidly passes from the fluctuating state to the frozen clus-

ter state and remains trapped for further times with only minor rearrangements. The frozen cluster state can be regarded as a solid that only breaks or melts once a critical level of thermal fluctuations is added. For increasing  $F^T$ , the behavior becomes increasingly intermittent. A frozen cluster forms for a period of time but can undergo an instability that sends the system back into a fluctuating state for another period of time before a new frozen cluster appears. This process is illustrated in Fig. 6(c,g) for  $F^T = 6.0$ , where the regions of strongly fluctuating  $V(t)$  are correlated with strongly fluctuating values of  $P_6(t)$ . We do not observe this type of two-step intermittent behavior in the fluctuating regime at  $\phi < \phi_c$  for  $F^T = 0$ . The higher temperature systems no longer become permanently absorbed into the frozen state; instead, we observe temperature-induced transitions for  $\phi > \phi_c$  from the frozen state at low temperature to the intermittent state at intermediate temperatures. When the stochastic fluctuations are large enough the system always remains in the fluctuating state, as shown in Fig. 6(d,h) for  $F^T = 9.0$ . The value of  $F^T$  at which the system remains permanently in a fluctuating state decreases with decreasing  $\phi/\phi_c$ . These results show that the transition to the dynamically frozen state can still be realized in the presence of fluctuations provided the additional stochastic fluctuations are sufficiently small.

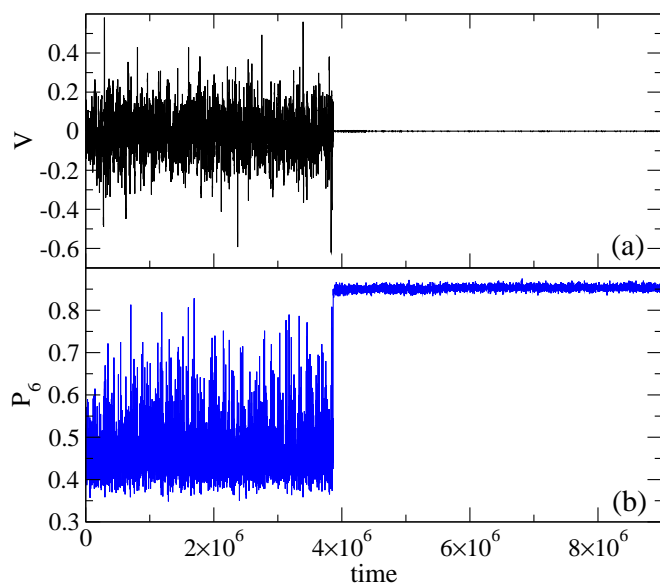


**Fig. 7** (a)  $V(t)$  for a system at  $\phi = 0.363$  containing  $N_p = 2$  obstacles or pinned disks. (b) The corresponding  $P_6(t)$ . Even though  $\phi < \phi_c$ , the system shows a transition to a dynamically frozen state consisting of a pinned cluster.

## 6 Dynamic Freezing in the Presence of Obstacles

We next consider the effects of adding a small number of obstacles to the system in form of stationary or pinned disks. In this case we find that even a very low obstacle density can cause the system to organize into a dynamic frozen state at values of  $\phi$  well below the obstacle-free critical value  $\phi_c$ ; however, the nature of the frozen states in the presence and absence of obstacles are quite different. Figure 7(a) shows  $V(t)$  for a system at  $\phi = 0.363$  containing  $N_p = 2$  obstacles. There is a clear transition from a fluctuating state to a dynamically frozen state even though  $\phi < \phi_c$ . The corresponding  $P_6(t)$  in Fig. 7(b) shows large variations in the fluctuating state with values as large as  $P_6 = 0.81$  indicating transient clustering, while at the transition to the frozen state we find  $P_6 \approx 0.84$  as the system forms a pinned hexagonal-faceted crystal that is centered near one of the obstacles.

The obstacles serve as cluster nucleation sites. Figure 8 shows snapshots at different times of the disk and obstacle positions for the system in Fig. 7. In the initial fluctuating state in Fig. 8(a), there are small transient clusters. Figure 8(b) shows the system at a later time but still in the fluctuating state where a cluster nucleates around one of the obstacles. This cluster eventually breaks apart as illustrated in Fig. 8(c) which shows an even later time in the fluctuating state. Figure 8(d) shows the configuration in the dynamically frozen state where a faceted crystal forms around the obstacles.

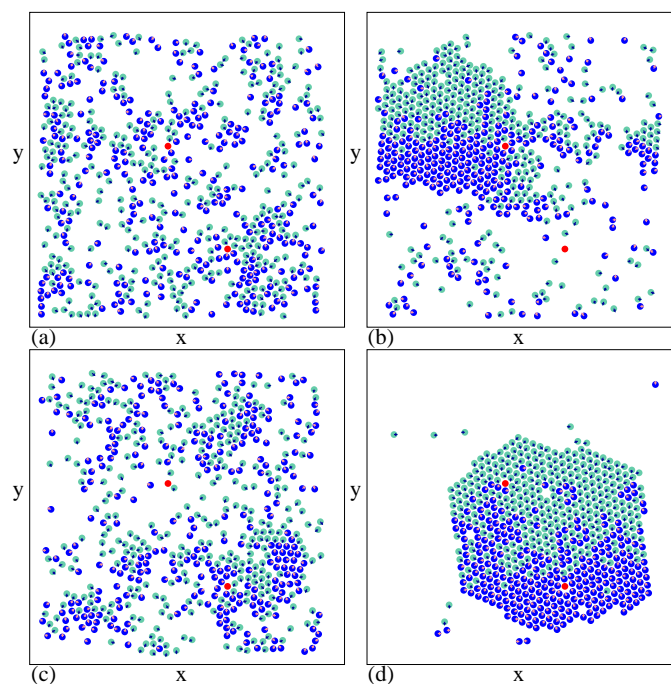


**Fig. 8** Snapshots of disk and obstacle positions in a system with  $\phi = 0.363$  and  $N_p = 2$  where the arrows indicate the direction of the motor force for each disk. Moving disks are colored as in Fig. 4. Red disks are immobile obstacles. (a) The initial fluctuating state containing small transient clusters. (b) At a later time, transient clusters are nucleated by the obstacles. (c) At a still later time, the transient cluster shown in (b) has broken apart. (d) The dynamically frozen steady state where a faceted crystal forms around the obstacles.

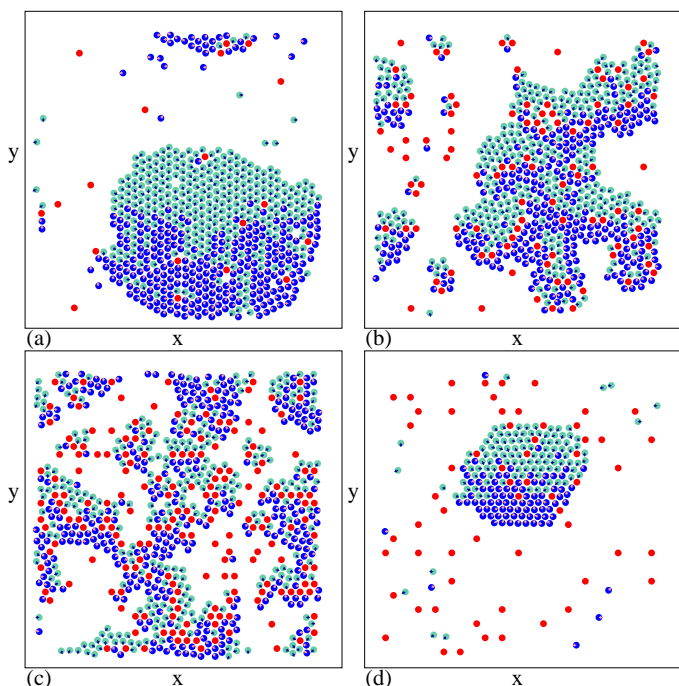


**Fig. 9** Snapshots of disk and obstacle positions in dynamically frozen states of systems containing obstacles where the arrows indicate the direction of the motor force for each disk. Moving disks are colored as in Fig. 4. Red disks are immobile obstacles. (a) At  $\phi = 0.363$  and  $N_p = 20$ , the cluster no longer has facets. (b) At  $\phi = 0.363$  and  $N_p = 100$ , the cluster starts to become much more disordered. (c) At  $\phi = 0.363$  and  $N_p = 200$ , multiple clusters start to form. (d) At  $\phi = 0.1212$  and  $N_p = 60$  cluster formation still occurs.

steady state, where the particles form a single cluster that has the shape of a faceted hexagonal crystal. Unlike the frozen steady state in the obstacle-free system, the cluster in Fig. 8(d) is not drifting but is pinned by the obstacles. The cluster exhibits the additional feature that the particles in the upper half of the cluster are moving in the negative  $y$  direction on average while the particles in the lower half of the cluster are moving in the positive  $y$  direction on average. In particular, the particles on the outer edges of the crystal have their motor forces oriented toward the center of the cluster. There are a small number of particles outside of the cluster that are moving in closed orbits.

In general for  $\phi < \phi_c$ , when a small number of obstacles are present the system eventually forms a faceted pinned crystal centered around the defects. When more obstacles are added, the transient time to reach the pinned state decreases and the system may form multiple pinned clusters. In Fig. 9(a), a system with  $\phi = 0.363$  and  $N_p = 20$  forms a single cluster that no longer has the faceted features found for lower obstacle

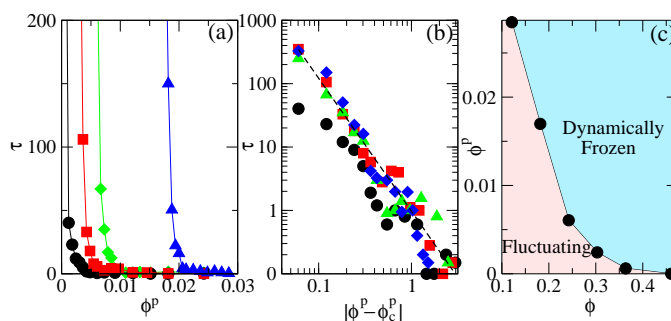


**Fig. 10** (a) The transient time  $\tau$  to reach a pinned cluster state vs the obstacle density  $\phi^p$  for  $\phi = 0.363$  (circles),  $0.303$  (squares),  $0.2424$  (diamonds), and  $0.182$  (triangles). (b) A log-log plot of  $\tau$  vs  $|\phi^p - \phi_c^p|$ , where the solid line is a fit to  $\tau \propto |\phi^p - \phi_c^p|^{-\beta}$  with  $\beta = 1.9$ . (c)  $\phi_p$  vs  $\phi$  showing the separation between the region where the system remains fluctuating and the dynamically frozen region where the system eventually forms a pinned cluster state.

densities. Adding more obstacles to the same system produces the frozen steady state shown in Fig. 9(b), where the clustering is much more disordered when  $N_p = 100$ . Figure 9(c) shows the same system with  $N_p = 200$ , where multiple pinned clusters form. The cluster states can also occur at lower densities, as illustrated in Fig. 9(d) for a system with  $\phi = 0.1212$  and  $N_p = 60$ .

For  $\phi < \phi_c$  we find that there is a critical obstacle density  $\phi_c^p$  below which the system never reaches a dynamically frozen steady state. In Fig. 10(a) we plot the transient time  $\tau$  required to reach a pinned cluster versus the obstacle density  $\phi^p$  for  $\phi = 0.363, 0.303, 0.2424$ , and  $0.182$ , showing that  $\tau$  diverges at differing critical pinning densities  $\phi_c^p$ . The curves can be fit to the form  $\tau \propto |\phi^p - \phi_c^p|^{-\beta}$  with  $\beta \approx 1.9 \pm 0.4$ , as shown in the log-log plot of Fig. 10(b). The fact that the transition from the fluctuating to the dynamical state shows a different scaling than in the obstacle-free case suggests that the addition of obstacles changes the class of the transition. In Fig. 10(c) we show the line dividing the dynamically frozen and fluctuating steady states on a plot of obstacle density  $\phi^p$  versus disk density  $\phi$ . As  $\phi$  decreases, the density of obstacles required to induce the formation of a dynamically frozen state increases.

There have been several studies examining the effect of quenched disorder on active matter systems. For flocking models it was found that the coherence of the system passes through a maximum when random noise is added<sup>56,57</sup>. For run and tumble dynamics it was shown that the effective mobility decreases with increasing run length<sup>58</sup>. In both classes of system, a fluctuating state is always present, so there is not a sharp transition to a completely pinned state as we observe in this work.



## 7 Summary

We examine a system of run-and-tumble disks in the limit of infinite run time and find that above a critical density, a transition occurs from a fluctuating state to an absorbing quiescent state. In the dynamically frozen state, a drifting cluster forms and the fluctuations in the system almost completely vanish. The transient time required for the system to organize into the dynamically frozen state diverges as a power law as the critical density is approached with an exponent of  $\nu_{||} \approx 1.21$ . This behavior is very similar to that observed in the random organization transition to a non-fluctuating state in sheared colloidal systems where the transient times also show power law divergences with comparable critical exponents. A key difference between the random organization and active matter systems is that in the quiescent state, the colloidal particles cease to interact with each other, while the active matter particles form a strongly correlated or jammed configuration in which most of the particles are in constant contact. We also find that the magnitude of the fluctuations diverge as  $\phi_c$  is approached from below. The dynamic transition is robust against the addition of a certain range of stochastic or thermal fluctuations. When a small number of obstacles are added to the system, the transition to a frozen state can occur at densities much lower than the obstacle-free critical density, and in this case the frozen state is characterized by the formation of pinned faceted crystals.

## 8 Acknowledgements

This work was carried out under the auspices of the NNSA of the U.S. DoE at LANL under Contract No. DE-AC52-06NA25396.

## References

- 1 H. Hinrichsen, *Adv. Phys.*, 2000, **49**, 815.
- 2 S. Lübeck and P.C. Heger, *Phys. Rev. E*, 2003, **68**, 056102.
- 3 A.K. Takeuchi, *J. Stat. Mech.*, 2014, **2014**, P01006.
- 4 D.J. Pine, J.P. Gollub, J.F. Brady, and A.M. Leshansky, *Nature (London)*, 2005, **438**, 997.
- 5 L. Corté, P.M. Chaikin, J.P. Gollub, and D.J. Pine, *Nature Phys.*, 2008, **4**, 420.
- 6 G.I. Menon and S. Ramaswamy, *Phys. Rev. E*, 2009, **79**, 061108.
- 7 A. Franceschini, E. Filippidi, E. Guazzelli, and D.J. Pine, *Phys. Rev. Lett.*, 2011, **107**, 250603.
- 8 K.A. Takeuchi, M. Kuroda, H. Chaté, and M. Sano, *Phys. Rev. Lett.*, 2007, **99**, 234503.
- 9 H. Hinrichsen, A. Jimenez-Dalmaroni, Y. Rozov, and E. Domany, *Phys. Rev. Lett.*, 1999, **83**, 4999.
- 10 V. Narayan, S. Ramaswamy, and N. Menon, *Science*, 2007, **317**, 105.
- 11 N. Mangan, C. Reichhardt, and C.J. Olson Reichhardt, *Phys. Rev. Lett.*, 2008, **100**, 187002.
- 12 S. Okuma, Y. Tsugawa, and A. Motohashi, *Phys. Rev. B*, 2011, **83**, 012503.
- 13 S. Ramaswamy, *Annu. Rev. Condens. Matter Phys.*, 2010, **1**, 323.
- 14 V. Schaller, C.A. Weber, B. Hammerich, E. Frey, and A.R. Bausch, *Proc. Natl. Acad. Sci. (USA)*, 2011, **108**, 19183.
- 15 C. Reichhardt and C.J. Olson Reichhardt, *Proc. Natl. Acad. Sci. (USA)*, 2011, **108**, 19099.
- 16 M.C. Marchetti, J.F. Joanny, S. Ramaswamy, T.B. Liverpool, J. Prost, M. Rao, and R.A. Simha, *Rev. Mod. Phys.*, 2013, **85**, 1143.
- 17 P. Grassberger and Y.-C. Zhang, *Physica A*, 1996, **224**, 169.
- 18 L. Milz and M. Schmiedeberg, *Phys. Rev. E*, 2013, **88**, 062308.
- 19 C.F. Schreck, R.S. Hoy, M.D. Shattuck, and C.S. O'Hern, *Phys. Rev. E*, 2013, **88**, 052205.
- 20 R. Moebius and C. Heussinger, arXiv:1404.1818.
- 21 D. Fiocco, G. Foffi, and S. Sastry, *Phys. Rev. E*, 2013, **88**, 020301.
- 22 I. Regev, T. Lookman, and C. Reichhardt, *Phys. Rev. E*, 2013, **88**, 062401.
- 23 N.C. Keim and P.E. Arratia, *Phys. Rev. Lett.*, 2014, **112**, 028302.
- 24 K.H. Nagamanasa, S. Gokhale, A.K. Sood, and R. Ganapathy, arXiv:1402.2730.
- 25 M.E. Cates, *Rep. Prog. Phys.*, 2012, **75**, 042601.
- 26 H.C. Berg, *E. coli in Motion* (Springer, New York, 2004).
- 27 J. Tailleur and M.E. Cates, *Phys. Rev. Lett.*, 2008, **100**, 218103.
- 28 M.B. Wan, C.J. Olson Reichhardt, Z. Nussinov, and C. Reichhardt, *Phys. Rev. Lett.*, 2008, **101**, 018102.
- 29 A.G. Thompson, J. Tailleur, M.E. Cates, and R.A. Blythe, *J. Stat. Mech.*, 2011, **2011**, P02029.
- 30 R. Di Leonardo, D. DellArciprete, L. Angelani, and V. Iebba, *Phys. Rev. Lett.*, 2011, **106**, 038101.
- 31 T. Vicsek, A. Czirok, E. Ben-Jacob, I. Cohen, and O. Shochet, *Phys. Rev. Lett.*, 1995, **75**, 1226.
- 32 J.A. Drocco, C.J. Olson Reichhardt, and C. Reichhardt, *Phys. Rev. E*, 2012, **85**, 056102.
- 33 D. Helbing, *Rev. Mod. Phys.*, 2011, **73**, 1067.
- 34 J.R. Howse, R.A.L. Jones, A.J. Ryan, T. Gough, R. Vafabakhsh, and R. Golestanian, *Phys. Rev. Lett.*, 2007, **99**, 048102.
- 35 J. Palacci, C. Cottin-Bizonne, C. Ybert, and L. Bocquet, *Phys. Rev. Lett.*, 2010, **105**, 088304.
- 36 B. ten Hagen, S. van Teeffelen, and H. Löwen, *J. Phys.: Condens. Matter*, 2011, **23**, 194119.
- 37 J. Palacci, S. Sacanna, A.P. Steinberg, D.J. Pine, and P.M. Chaikin, *Science*, 2013, **339**, 936.
- 38 M. E. Cates and J. Tailleur, *EPL*, 2013, **101**, 20010.
- 39 F. Kümmel, B. ten Hagen, R. Wittkowski, I. Buttinoni, R. Eichhorn, G. Volpe, H. Löwen, and C. Bechinger, *Phys. Rev. Lett.*, 2013, **110**, 198302.
- 40 A. Bricard, J.-B. Caussin, N. Desreumaux, O. Dauchot, and D. Bartolo, *Nature (London)*, 2013, **503**, 95.
- 41 S. Henkes, Y. Fily, and M.C. Marchetti, *Phys. Rev. E*, 2011, **84**, 040301.
- 42 J. Bialke, T. Speck, and H. Löwen, *Phys. Rev. Lett.*, 2012, **108**, 168301.
- 43 Y. Fily and M.C. Marchetti, *Phys. Rev. Lett.*, 2012, **108**, 235702.
- 44 G. Redner, M. Hagan, and A. Baskaran, *Phys. Rev. Lett.*, 2013, **110**, 055701.
- 45 B.M. Mognetti, A. Saric, S. Angioletti-Uberti, A. Cacciuto, C. Valeriani, and D. Frenkel, *Phys. Rev. Lett.*, 2013, **111**, 245702.
- 46 Y. Fily, S. Henkes, and M.C. Marchetti, *Soft Matter*, 2014, **10**, 2132.
- 47 D. Levis and L. Berthier, *Phys. Rev. E* **89**, 062301 (2014).
- 48 O. Pohl and H. Stark, *Phys. Rev. Lett.* **112**, 238303 (2014).
- 49 L. Berthier and J. Kurchan, *Nature Phys.*, 2013, **9**, 310.
- 50 N.H.P. Nguyen, D. Klotsa, Daphne, M. Engel, and S.C. Glotzer, *Phys. Rev. Lett.*, 2014, **112**, 075701.
- 51 M.B. Weissman, *Annu. Rev. Mater. Sci.*, 1996, **26**, 395.
- 52 M.W. Rabin, R.D. Merithew, M.B. Weissman, M.J. Higgins, and S. Bhat-tacharya, *Phys. Rev. B*, 1998, **57**, R720.
- 53 C.J. Olson, C. Reichhardt, and F. Nori, *Phys. Rev. Lett.*, 1998, **81**, 3757.

- 
- 54 C. Reichardt and C. J. Olson Reichardt, *Phys. Rev. Lett.*, 2004, **93**, 176405.
- 55 Z. Chen and C.C. Yu, *Phys. Rev. Lett.*, 2007, **98**, 057204.
- 56 O. Chepizhko, E.G. Altmann, and F. Peruani, *Phys. Rev. Lett.*, 2013, **110**, 238101.
- 57 O. Chepizhko and F. Peruani, *Phys. Rev. Lett.*, 2013, **111**, 160604.
- 58 C. Reichardt and C.J. Olson Reichardt, arXiv:1402.3260.